Coulomb Instabilities of a Three-Dimensional Higher-Order Topological Insulator

Peng-Lu Zhao,[1,2] Xiao-Bin Qiang,[1,2] Hai-Zhou Lu,[1,2,*] and X. C. Xie[3,4,5]

[1]*Shenzhen Institute for Quantum Science and Engineering and Department of Physics, Southern University of Science and Technology (SUSTech), Shenzhen 518055, China*
[2]*Shenzhen Key Laboratory of Quantum Science and Engineering, Shenzhen 518055, China*
[3]*International Center for Quantum Materials, School of Physics, Peking University, Beijing 100871, China*
[4]*CAS Center for Excellence in Topological Quantum Computation, University of Chinese Academy of Sciences, Beijing 100190, China*
[5]*Beijing Academy of Quantum Information Sciences, West Building 3, No. 10, Xibeiwang East Road, Haidian District, Beijing 100193, China*

(Received 10 May 2021; accepted 16 September 2021; published 18 October 2021)

Topological insulators (TIs) are an exciting discovery because of their robustness against disorder and interactions. Recently, second-order TIs have been attracting increasing attention, because they host topologically protected 1D hinge states in 3D or 0D corner states in 2D. A significantly critical issue is whether the second-order TIs also survive interactions, but it is still unexplored. We study the effects of weak Coulomb interactions on a 3D second-order TI, with the help of renormalization-group calculations. We find that the 3D second-order TIs are always unstable, suffering from two types of topological phase transitions. One is from second-order TI to TI, the other is to normal insulator. The first type is accompanied by emergent time-reversal and inversion symmetries and has a dynamical critical exponent $\kappa = 1$. The second type does not have the emergent symmetries but has nonuniversal dynamical critical exponents $\kappa < 1$. Our results may inspire more inspections on the stability of higher-order topological states of matter and related novel quantum criticalities.

DOI: 10.1103/PhysRevLett.127.176601

Introduction.—As generalizations of the topological insulators (TIs) [1–12], higher-order TIs have been attracting considerable interest recently [13–30]. A simplest 3D second-order TI hosts 3D gapped bulk states inside but topologically protected gapless 1D hinge states and gapped 2D surface states (Fig. 1). There have been experimental evidences for the higher-order topology in bosonic systems, including circuitry [31–33], phononics [34], acoustics [35–37], and photonics [38–41]. Despite the theoretical predictions on material candidates [18,19,42–45], there are few observations of higher-order TIs in electronic systems [19]. This raises concerns about the stability of higher-order TIs against, e.g., disorder [46–49]. More importantly, it is still unknown whether higher-order TIs can survive a more intrinsic presence in electronic systems, the Coulomb interactions [49–61].

In this Letter, we study the stability of 3D second-order TIs in the presence of the Coulomb interaction. We find that the second-order TIs are always unstable. Two types of topological phase transitions could happen (Fig. 1). In the first type, a topological phase transition from second-order TI to TI happens in the presence of the Coulomb interaction. This transition is accompanied and protected by the emergent time-reversal and inversion symmetries in the low-energy limit. The quantum criticality for this phase transition is described by a dynamical critical exponent $\kappa = 1$ and a correlation length exponent $\nu = 1$. In the second type, the Coulomb interaction could induce another topological phase transition from a second-order TI to a normal insulator (NI). There is no emergent symmetry when this phase transition happens, and its criticality is

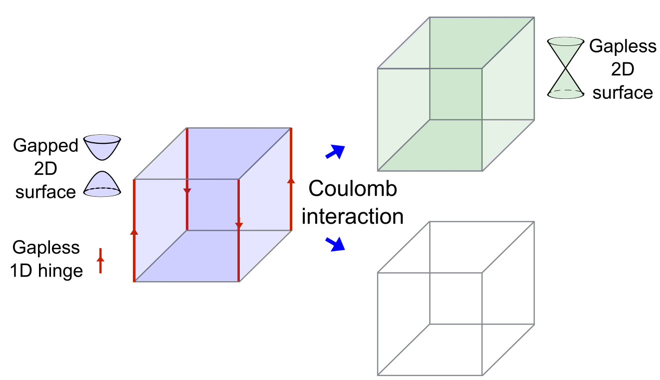

FIG. 1. Schematic of a typical 3D second-order TI (left) that hosts 3D gapped bulk states in the interior but topologically protected 2D massive (gapped) Dirac cones on the surfaces and gapless 1D chiral hinge states. It may turn to a TI (right top) or a NI (right bottom) in the presence of the Coulomb interactions.

characterized by the appearance of nonuniversal dynamical critical exponents $\kappa < 1$. Our results will be insightful for the ongoing experimental search for higher-order TIs in electronic systems.

Model for 3D second-order TIs.—We start with a four-band Hamiltonian for 3D second-order TIs [18],

$$\mathcal{H}_0(\mathbf{k}) = \left[M + \sum_i t_i \cos(ak_i)\right]\tau_z\sigma_0 + \sum_i \Delta_i \sin(ak_i) \times \tau_x\sigma_i + \Delta_2[\cos(ak_x) - \cos(ak_y)]\tau_y\sigma_0, \quad (1)$$

where $i = x, y, z$, a is the lattice constant, and σ_i and τ_i are the Pauli matrices. M, t_i, Δ_i, Δ_2 are the hopping parameters, and we take $t_x = t_y = t_\perp$, and $\Delta_x = \Delta_y = \Delta_\perp$. This model has no time-reversal symmetry if $\Delta_2 \neq 0$ (see Supplemental Material, Sec. SI [62]). A fourfold rotation symmetry $R_{4z} \equiv \tau_0 e^{-i(\pi/4)\sigma_z}$ is broken by the nonzero Δ_2 term. The combination $R_{4z}\mathcal{T}$ ($\mathcal{T}$ is the time-reversal operator) is a symmetry that protects the 3D second-order TIs. Another important symmetry is the combination of time reversal and inversion $\mathcal{IT}$ (Supplemental Material, Sec. SII [62]), where $\mathcal{I} = \tau_z\sigma_0$, with which the $\mathcal{Z}_2$ invariants are identified by

$$(-1)^\vartheta = \prod_i \prod_{n=1}^{N/2} \xi_n(\Gamma_i), \quad (2)$$

where $\xi_n(\Gamma_i) = \pm 1$ is the eigenvalue of $\mathcal{I}$ for the nth occupied energy band at momenta Γ_i, and $\Gamma_i \in \{(0,0,0), (\pi,\pi,0), (0,0,\pi), (\pi,\pi,\pi)\}$ representing all the $R_{4z}\mathcal{T}$-invariant $\mathbf{k}$ points. As a result, for $|2t_\perp - t_z| < |M| < |2t_\perp + t_z|$, $(-1)^\vartheta = -1$ (Supplemental Material, Sec. SII [62]), which represents the second-order TI and for $|M| > |2t_\perp + t_z|$ or $|M| < |2t_\perp - t_z|$, $(-1)^\vartheta = 1$, which stands for a NI. This difference establishes only when $\Delta_i \neq 0 \neq \Delta_2$. Once $\Delta_i = 0$, there exist gapless points that break the insulating nature. Once $\Delta_2 = 0$, time-reversal symmetry recovers and the phase is a TI. Below, we show that, even if starting with $\Delta_2 \neq 0$ and $|2t_\perp - t_z| < |M| < |2t_\perp + t_z|$, Δ_2 flows to zero in the low-energy limit in the presence of the Coulomb interaction, leading to a transition from second-order TI to TI, or causes $|M| > |2t_\perp + t_z|$, which induces a transition from second-order TI to NI.

Coulomb interaction and renormalization-group equations.—The effective action in Euclidean spacetime for the second-order TI in the presence of the Coulomb interaction takes the form (Supplemental Material, Sec. SIIIA [62])

$$\mathcal{S} = \int d\tau d^3\mathbf{r}\{\bar{\psi}[(\partial_\tau + ig\phi)\gamma_0 + v_i\gamma_i\partial_i + m + B_i\partial_i^2 - iD(\partial_x^2 - \partial_y^2)\gamma_5]\psi + \frac{1}{2}\eta_i(\partial_i\phi)^2\}, \quad (3)$$

where ψ describes a four-component fermion field and $\bar{\psi} = \psi^\dagger\gamma_0$. The γ matrices satisfy the anticommuting algebra $\{\gamma_\mu, \gamma_\nu\} = 2\delta_{\mu,\nu}$. The repeated index i sums for $i = x, y, z$, and $v_i = \Delta_i a$, $m = M + 2t_\perp + t_z$, $B_i = t_i a^2/2$, and $D = \Delta_2 a^2/2$, which are obtained by expanding Eq. (1) around the Γ point. The parameter m is the Dirac mass, and the B_i and D terms represent the quadratic corrections to the Dirac Hamiltonian. We introduce an auxiliary scale field ϕ through the Hubbard-Stratonovich transformation [63] to decouple the density-density Coulomb interaction. $(\eta_x, \eta_y, \eta_z) = (1, 1, \eta)$ characterize the spatial anisotropy of ϕ. $g = e/\sqrt{\epsilon}$ represents the coupling between electrons and the scalar field, where $-e$ is the electron charge and ϵ is the dielectric constant. The Coulomb interaction does not break the $R_{4z}\mathcal{T}$ and $\mathcal{IT}$ symmetries of Eq. (1) (Supplemental Material, Sec. SIIIA [62]), and the topology is still distinguished by Eq. (2). The noninteracting invariant for interacting systems has been justified in [18,68]. According to Eq. (1), m controls the gap [3,9,69]. Its sign identifies the phase transition between a second-order TI and NI.

To explore how the Coulomb interaction renormalizes the parameters and consequently leads to the phase transitions, we perform a Wilsonian momentum-shell renormalization-group analysis [64,70] for Eq. (3). We redefine the original parameters B_i, D, m, and v_i and Coulomb interaction strength g into dimensionless

$$\begin{aligned} \text{quadratic terms:} \quad & B_i\Lambda v^{-1}\eta_i^{-1} \to B_i, \qquad D\Lambda v^{-1} \to D, \\ \text{anisotropy:} \quad & \gamma^2 = v_z/(v\eta), \\ \text{gap:} \quad & mv^{-1}\Lambda^{-1} \to m, \\ \text{Coulomb:} \quad & g^2/(4\pi^2 v\sqrt{\eta}) \to \alpha, \end{aligned} \quad (4)$$

where Λ is the cutoff, $v = v_{x,y}$. The renormalization-group flow equations for them can be found in the Supplemental Material, Sec. SIIIC [62]. We numerically solve these renormalization-group equations and obtain the running of m, B_i, D, α, and γ^2 with ℓ, where ℓ is the running scale parameter whose value increase lowers the energy scale. Despite the fact that the running of these parameters highly depends on their initial values at the cutoff Λ, their behaviors can be classified into two types of phase transitions.

From second-order TI to TI.—This phase transition is characterized by a vanishing D without a sign change of m at large ℓ (low energy). Figure 2(a) shows that, in a large range of D_0, D flows to zero rapidly with increasing ℓ. This behavior reflects the fact that the renormalization-group equation for D [Supplemental Material [62], Eq. (S112)] only has one stable fixed point at $D_* = 0$. As D flows to zero, m increases and remains positive [Fig. 2(b)]. The unrestricted growth of m ceases the rapid decay of α [Fig. 2(c)]. Although the effective Coulomb interaction is marginally irrelevant [Supplemental Material [62],

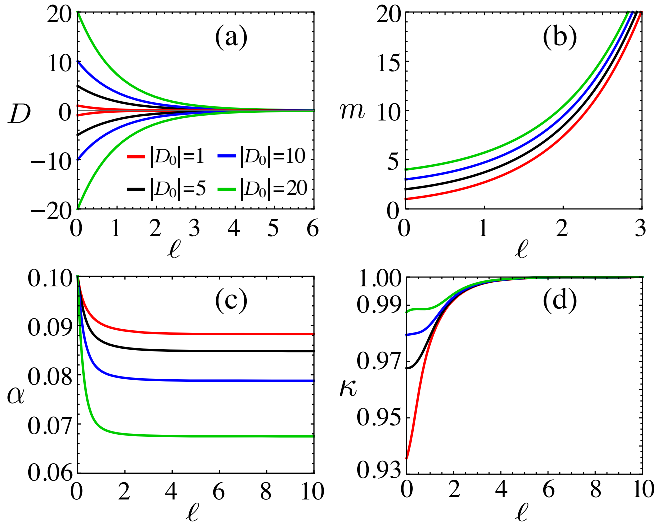

FIG. 2. (a)–(c) The renormalized D, m, and α as functions of the running scale parameter ℓ. D and m protect the second- and first-order topological properties, respectively. The vanishing D and increasing m mean a topological phase transition from second-order TI to TI. (d) The scale dependence of the dynamic exponent κ, whose value is obtained by fixing v as scale invariant. The solutions are obtained by fixing the initial values $m_0 = B_\perp^0 = 1$, $B_z^0 = 0.5$, $\alpha_0 = 0.1 = \gamma_0^2 = 0.1$ while varying D_0. (a)–(d) share the same legends. In (b), the $m(\ell)$ curves of $D_0 = 5$, 10, and 20 are shifted vertically by 1 for clarity.

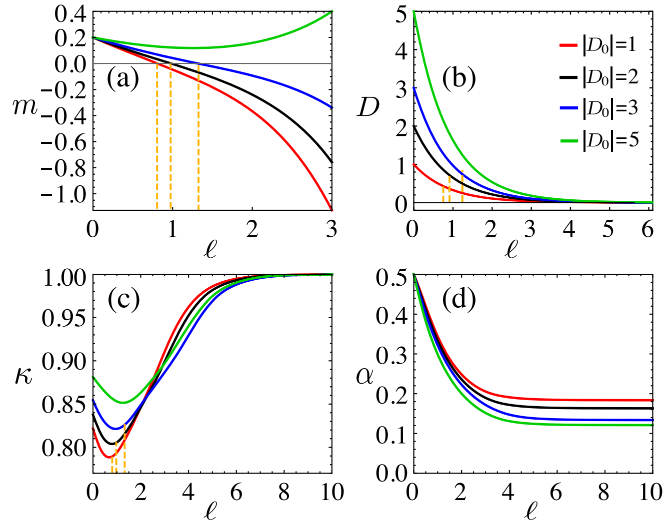

FIG. 3. (a),(b),(d) The renormalized m, D, and α as functions of the running scale parameter ℓ. D and m protect the second-order and first-order topological properties, respectively. The finite D at the sign change of m means a topological phase transition from 3D second-order TI to NI. (c) The scale dependence of κ. The solutions are obtained by varying the initial value of D while fixing those of other parameters as $m_0 = 0.2$, $B_\perp^0 = 2B_z^0 = 2$, $\alpha_0 = 0.5$, and $\gamma_0^2 = 0.1$. (a)–(d) Legends are the same. The orange dashed lines in (a)–(c) label the values of ℓ at the phase transition points. (b),(c) The crossing points of the orange dashed lines with the red, black, blue lines indicate the values of D and κ when the phase transition occurs. From left to right, $D = 0.43$, 0.72, 0.74 in (b) and $\kappa = 0.79$, 0.81, 0.83 in (c).

Eq. (S113)], its value in the low-energy limit is a small constant instead of zero [see Fig. 2(c)]. With no sign change of m, there is no gap closing and reopening near the Γ point when approaching the low-energy limit, and the topological invariant does not change. However, when D flows to zero, the free part of the effective model (3) reduces to the modified Dirac Hamiltonian that describes TIs [7,9]. According to the previous results [51,71–73], TIs are immune to weak Coulomb interactions. Therefore, the low-energy state is a TI with finite but weak Coulomb interactions, which means that the second-order TI is unstable to the Coulomb interaction. After the transition from the second-order TI to TI, the hinge modes disappear only because the surface gaps close, so it does not require a gap closing of the 3D bulk states. Time-reversal symmetry and inversion symmetry emerge along with the phase transition. Previous works have shown the possibilities of emergent Lorentz symmetry [74–81], chiral symmetry [82–84], and supersymmetry [85–96]. Our concrete example above shows the emergent discrete time-reversal and inversion symmetries, enriching the family of emergent symmetries [97]. This phase transition does not need a large critical value of α and exists at least for $\alpha \sim 10^{-3}$, corresponding to an extremely weak Coulomb interaction (Supplemental Material, Sec. IV [62]). We find that the dynamical critical exponent $\kappa = 1$ for this phase transition, as shown in Fig. 2(d). We also obtain a correlation length exponent $\nu = 1$ by assuming that the spatial correlation length ξ diverges as $\delta \equiv D - D_* \to 0$ in the manner of $\xi \sim |\delta|^{-\nu}$. This definition is similar to the conventional definition of the correlation length exponent in a symmetry-broken quantum phase transition [98,99].

From second-order TI to NI.—This phase transition is characterized by a sign change of m and a finite D as m changes sign. Here, the finite D guarantees that the topological phase transition to NI happens before the transition to TI. Figure 3(a) shows that m changes sign when D_0 is below a critical value. For comparison, the green line shows a case in which m does not change sign. Figure 3(b) shows that D does not vanish when m changes sign. Therefore, for the parameters represented by the red, black, and blue lines in Fig. 3(a), the transitions from second-order TI to NI happen and for the case depicted by the green line the transition from second-order TI to TI happens. After the transition from the second-order TI to NI, both the hinge and surface modes disappear. Because of the finite D, there are no emergent time-reversal and inversion symmetries at the phase transition point. After the transition, these two emergent symmetries appear in the low-energy limit of the NI. Interestingly, this transition has no universal dynamical critical exponent. Figure 3(c) shows that the dynamical critical exponent has different values for the three cases, all below 1. A nonuniversal $\kappa < 1$ is a direct result of the transition happening at a finite energy scale ℓ. By fixing the fermion velocities as scale invariant, we obtain

$$\kappa(\ell) = 1 - \alpha(\ell)\mathcal{F}_0^{\perp}(\ell), \quad (5)$$

where $\mathcal{F}_0^{\perp}$ is a dimensionless function of m, B_i, D, and γ^2 whose expression is given by Eq. (S36) in the Supplemental Material [62]. The values of $\alpha(\ell)$ are always positive constants [see Fig. 3(d)], and the non-negative $\mathcal{F}_0^{\perp}(\ell)$ vanishes only as $\ell \to \infty$. Considering that the sign change of m always happens at a finite ℓ, the value of κ is smaller than 1 and its particular value depends on α and $\mathcal{F}_0^{\perp}(\ell)$, and hence it is nonuniversal. However, as shown in Fig. 3(c), the asymptotic value of κ as $\ell \to \infty$ is still 1, which describes the low-energy dynamics of the NI. We have shown our main results by varying the initial value of D while fixing those of the other parameters. We could perform similar analyses for any cases by changing the initial value of one parameter while fixing others, but our conclusions still hold.

Screened Coulomb interaction.—The screening of Coulomb interaction cannot change our main conclusions. Because of the existence of gap m, once the Fermi energy is placed in the gap, the density of states vanishes. The screening effect is extremely weak (Supplemental Material, Sec. SVA [62]), compared to those in metals and semimetals, which implies that the treatment and conclusion are probably different for higher-order semimetals. Because of the weak screening effect, our conclusions also apply to large but not infinitely large-N flavors of fermions. This is different from the 2D gapless systems where the screening is strong and a large-N expansion was widely used to study the Coulomb effects [59,100,101].

Effect of coexisting disorder.—We introduce disorder described by $\delta H = U_i(x)\bar{\psi}\Gamma_i\psi$ [65–67], where Γ_i is a 4×4 Hermitian matrix and $U_i(x)$ is the impurity potential of a Gaussian white-noise distribution as $\langle U_i \rangle = 0$ and $\langle U_i(\mathbf{x})U_j(\mathbf{x}')\rangle = \Delta_i\delta_{ij}\delta(\mathbf{x}-\mathbf{x}')$. The types of disorder that respect $R_{4z}\mathcal{T}$ and $\mathcal{IT}$ symmetries are denoted by $\Gamma_i = \mathcal{I}_{4\times 4}$ and $\Gamma_i = \gamma_0$ (Supplemental Material, Sec. SVI [62]) and are dubbed the random mass and random chemical potential, respectively. The coupling strength Δ_M for the random mass is irrelevant [Fig. 4(a)] and hence it cannot prevent the phase transitions in the clean system. Figure 4(b) shows that the coupling strength Δ_C has a critical value Δ_C^c for the random chemical potential. Once the initial value Δ_C^0 is smaller than Δ_C^c, the random chemical potential is also irrelevant and cannot change our conclusions (Supplemental Material, Sec. SVI of [62]). The disorder-induced renormalization to the gap m shifts the boundaries between the two kinds of phase transitions. Figure 4(c) shows that the boundaries between the phase transition to TI and NI for systems without disorder, with random mass,

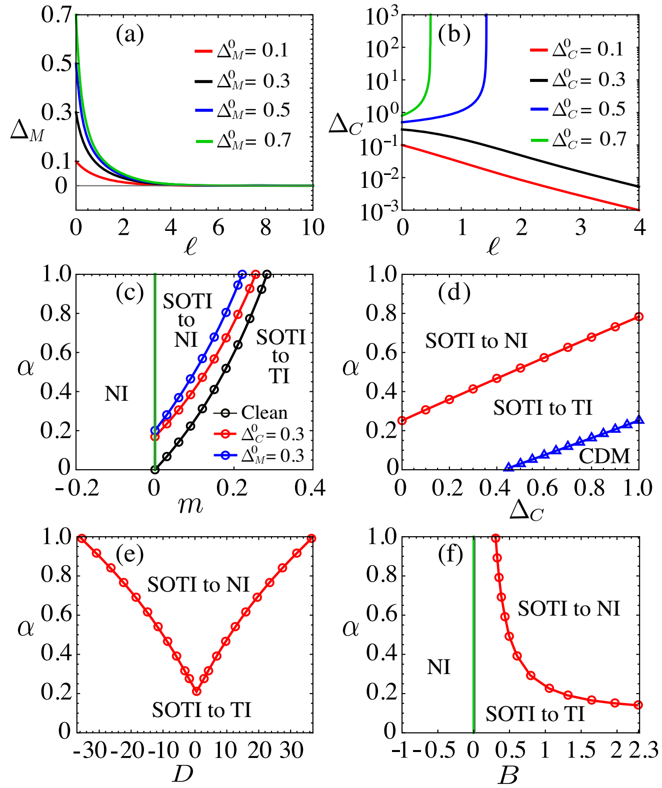

FIG. 4. (a),(b) The renormalized Δ_M and Δ_C. The different curves are obtained by fixing the initial values $m_0 = B_\perp^0 = B_z^0 = \gamma_0^2 = 0.1$, $\alpha_0 = 0.5$ while varying the initial values of Δ_M in (a) and Δ_C in (b). (c)–(f) Phase diagrams in the m–α, Δ_C–α, D–α, and B–α planes, respectively. SOTI and CDM stand for the second-order topological insulator and compressible diffusive metal, respectively. In (c), the black, red, and blue lines represent the boundaries for the cases without disorder, with random mass $\Delta_M^0 = 0.3$ and with random chemical potential $\Delta_C^0 = 0.3$, respectively. No disorder in (e) and (f). In (f), we take $B_\perp^0 = B_z = B$. The other parameters are fixed at (c)–(e) $B_\perp^0 = B_z^0 = 1$; (d)–(f) $m_0 = 0.1$; (c),(d),(f) $D_0 = 1$, 1, 0.1, respectively; $\gamma_0^2 = 0.1$ for all diagrams.

and with random chemical potential are different. If $\Delta_C^0 > \Delta_C^c$, a disorder-induced phase transition happens and the system flows to a disorder-dominated phase, dubbed the compressible diffusive metal [47,62]. There exist three phases in the $\Delta_C - \alpha$ plane, as shown in Fig. 4(d).

Phase diagrams.—To have a global view of the various phases, we show four phase diagrams on the planes of different parameters in Figs. 4(c)–4(f). According to Fig. 4(c), m plays a key role to determine the type of phase transition. Once m is large enough, the transition to NI cannot happen. Because of the dominant role of m, our conclusion also applies to other 3D second-order TIs (e.g., the helical second-order TI [18]), in particular, when the topology depends on the quadratic or higher-order corrections to the Dirac Hamiltonian (e.g., the D-term in our model). According to our calculation, these terms are all irrelevant in the low-energy limit, which causes the transition to TI. The transition from second-order TI to NI originates from the Coulomb-interaction-induced interplay between the anisotropic quadratic term (B_i) and gap (m), which does not depend on the terms protecting the second-order TIs and hence still exist for other 3D second-order TIs.

Discussion.—Our results show that the Coulomb interactions are critical in the experiments searching for higher-order TIs, even for weak Coulomb interactions. Stronger interactions may induce fractional higher-order topological phases or excitonic insulators, as those in the first-order topological phases [102–107].

Our theory shares a similar spirit as the transition between TI and NI in $BiTl(S_{1-\delta}Se_{\delta})_2$ [108] by varying δ. By fixing the parameters at the cutoff and analyzing their behaviors at a particular low-energy scale, the change of their initial values is equivalent to their changes at the particular energy scale relevant to the experiment. Therefore, the topological phase transitions from higher-order TI to NI or TI are possible in experiments using doping, such as the candidate materials bismuth [19], $EuIn_2As_2$ [44], and $MnBi_2Te_4$ [45], where the 1D gapless hinge states may transform to gapped states or 2D Dirac cone.

We thank helpful discussions with Jing-Rong Wang, Hao-Jie Lin, and Dao-Yuan Li. This work was supported by the National Natural Science Foundation of China (11925402 and 12047531), the National Basic Research Program of China (2015CB921102), the Strategic Priority Research Program of Chinese Academy of Sciences (XDB28000000), Guangdong province (2020KCXTD001 and 2016ZT06D348), Shenzhen High-level Special Fund (G02206304 and G02206404), and the Science, Technology and Innovation Commission of Shenzhen Municipality (ZDSYS20170303165926217, JCYJ20170412152620376, and KYTDPT20181011104202253). The numerical calculations were supported by Center for Computational Science and Engineering of SUSTech.

*Corresponding author.
luhz@sustech.edu.cn

[1] L. Fu, C. L. Kane, and E. J. Mele, Topological Insulators in Three Dimensions, Phys. Rev. Lett. **98**, 106803 (2007).
[2] J. E. Moore and L. Balents, Topological invariants of time-reversal-invariant band structures, Phys. Rev. B **75**, 121306 (R) (2007).
[3] S. Murakami, Phase transition between the quantum spin Hall and insulator phases in 3D: Emergence of a topological gapless phase, New J. Phys. **9**, 356 (2007).
[4] R. Roy, Topological phases and the quantum spin Hall effect in three dimensions, Phys. Rev. B **79**, 195322 (2009).
[5] L. Fu and C. L. Kane, Topological insulators with inversion symmetry, Phys. Rev. B **76**, 045302 (2007).
[6] D. Hsieh, D. Qian, L. Wray, Y. Xia, Y. S. Hor, R. J. Cava, and M. Z. Hasan, A topological Dirac insulator in a quantum spin Hall phase, Nature (London) **452**, 970 (2008).
[7] H. Zhang, C.-X. Liu, X.-L. Qi, X. Dai, Z. Fang, and S.-C. Zhang, Topological insulators in Bi_2Se_3, Bi_2Te_3 and Sb_2Te_3 with a single Dirac cone on the surface, Nat. Phys. **5**, 438 (2009).
[8] Y. Xia, D. Qian, D. Hsieh, L. Wray, A. Pal, H. Lin *et al.*, Observation of a large-gap topological-insulator class with a single Dirac cone on the surface, Nat. Phys. **5**, 398 (2009).
[9] S.-Q. Shen, *Topological Insulators*, 2nd ed. (Springer-Verlag, Berlin, Heidelberg, 2017).
[10] M. Z. Hasan and C. L. Kane, Colloquium: Topological insulators, Rev. Mod. Phys. **82**, 3045 (2010).
[11] X.-L. Qi and S.-C. Zhang, Topological insulators and superconductors, Rev. Mod. Phys. **83**, 1057 (2011).
[12] M. Z. Hasan and J. E. Moore, Three-dimensional topological insulators, Annu. Rev. Condens. Matter Phys. **2**, 55 (2011).
[13] W. A. Benalcazar, B. A. Bernevig, and T. L. Hughes, Quantized electric multipole insulators, Science **357**, 61 (2017).
[14] W. A. Benalcazar, B. A. Bernevig, and T. L. Hughes, Electric multipole moments, topological multipole moment pumping, and chiral hinge states in crystalline insulators, Phys. Rev. B **96**, 245115 (2017).
[15] Z. Song, Z. Fang, and C. Fang, $(d-2)$-Dimensional Edge States of Rotation Symmetry Protected Topological States, Phys. Rev. Lett. **119**, 246402 (2017).
[16] C. M. Wang, H.-P. Sun, H.-Z. Lu, and X. C. Xie, 3D Quantum Hall Effect of Fermi Arcs in Topological Semimetals, Phys. Rev. Lett. **119**, 136806 (2017).
[17] J. Langbehn, Y. Peng, L. Trifunovic, F. von Oppen, and P. W. Brouwer, Reflection-Symmetric Second-Order Topological Insulators and Superconductors, Phys. Rev. Lett. **119**, 246401 (2017).
[18] F. Schindler, A. M. Cook, M. G. Vergniory, Z. Wang, S. S. P. Parkin, B. A. Bernevig, and T. Neupert, Higher-order topological insulators, Sci. Adv. **4**, eaat0346 (2018).
[19] F. Schindler, Z. Wang, M. G. Vergniory, A. M. Cook, A. Murani, S. Sengupta *et al.*, Higher-order topology in bismuth, Nat. Phys. **14**, 918 (2018).
[20] M. Ezawa, Higher-Order Topological Insulators and Semimetals on the Breathing Kagome and Pyrochlore Lattices, Phys. Rev. Lett. **120**, 026801 (2018).
[21] Z. Li, Y. Cao, P. Yan, and X. Wang, Higher-order topological solitonic insulators, npj Comput. Mater. **5**, 107 (2019).
[22] T. Liu, Y.-R. Zhang, Q. Ai, Z. Gong, K. Kawabata, M. Ueda, and F. Nori, Second-Order Topological Phases in Non-Hermitian Systems, Phys. Rev. Lett. **122**, 076801 (2019).
[23] X.-W. Luo and C. Zhang, Higher-Order Topological Corner States Induced by Gain and Loss, Phys. Rev. Lett. **123**, 073601 (2019).
[24] K. Kudo, T. Yoshida, and Y. Hatsugai, Higher-Order Topological Mott Insulators, Phys. Rev. Lett. **123**, 196402 (2019).

[25] R. Chen, C.-Z. Chen, J.-H. Gao, B. Zhou, and D.-H. Xu, Higher-Order Topological Insulators in Quasicrystals, Phys. Rev. Lett. **124**, 036803 (2020).
[26] A. Agarwala, V. Juricic, and B. Roy, Higher-order topological insulators in amorphous solids, Phys. Rev. Research **2**, 012067(R) (2020).
[27] H. Hu, B. Huang, E. Zhao, and W. V. Liu, Dynamical Singularities of Floquet Higher-Order Topological Insulators, Phys. Rev. Lett. **124**, 057001 (2020).
[28] B. Huang and W. V. Liu, Floquet Higher-Order Topological Insulators with Anomalous Dynamical Polarization, Phys. Rev. Lett. **124**, 216601 (2020).
[29] X. Li and W. V. Liu, Weyl semimetal made ideal with a crystal of Raman light and atoms, Science Bulletin **66**, 1253 (2021).
[30] B. Fu, Z.-A. Hu, and S.-Q. Shen, The bulk-hinge correspondence and three-dimensional quantum anomalous Hall effect in second order topological insulators, Phys. Rev. Research **3**, 033177 (2021).
[31] C. W. Peterson, W. A. Benalcazar, T. L. Hughes, and G. Bahl, A quantized microwave quadrupole insulator with topologically protected corner states, Nature (London) **555**, 346 (2018).
[32] S. Imhof, C. Berger, F. Bayer, J. Brehm, L. W. Molenkamp, T. Kiessling *et al.*, Topolectrical-circuit realization of topological corner modes, Nat. Phys. **14**, 925 (2018).
[33] M. Serra-Garcia, R. Süsstrunk, and S. D. Huber, Observation of quadrupole transitions and edge mode topology in an LC circuit network, Phys. Rev. B **99**, 020304(R) (2019).
[34] M. Serra-Garcia, V. Peri, R. Süsstrunk, O. R. Bilal, T. Larsen, L. G. Villanueva, and S. D. Huber, Observation of a phononic quadrupole topological insulator, Nature (London) **555**, 342 (2018).
[35] H. Xue, Y. Yang, F. Gao, Y. Chong, and B. Zhang, Acoustic higher-order topological insulator on a kagome lattice, Nat. Mater. **18**, 108 (2019).
[36] X. Ni, M. Weiner, A. Alù, and A. B. Khanikaev, Observation of higher-order topological acoustic states protected by generalized chiral symmetry, Nat. Mater. **18**, 113 (2019).
[37] H. Xue, Y. Ge, H. X. Sun, Q. Wang, D. Jia, Y. J. Guan, S. Q. Yuan, Y. Chong, and B. Zhang, Observation of an acoustic octupole topological insulator, Nat. Commun. **11**, 2442 (2020).
[38] S. Mittal, V. V. Orre, G. Zhu, M. A. Gorlach, A. Poddubny, and M. Hafezi, Photonic quadrupole topological phases, Nat. Photonics **13**, 692 (2019).
[39] A. El Hassan, F. K. Kunst, A. Moritz, G. Andler, E. J. Bergholtz, and M. Bourennane, Corner states of light in photonic waveguides, Nat. Photonics **13**, 697 (2019).
[40] B.-Y. Xie, G.-X. Su, H.-F. Wang, H. Su, X.-P. Shen, P. Zhan, M.-H. Lu, Z.-L. Wang, and Y.-F. Chen, Visualization of Higher-Order Topological Insulating Phases in Two-Dimensional Dielectric Photonic Crystals, Phys. Rev. Lett. **122**, 233903 (2019).
[41] M. Li, D. Zhirihin, M. Gorlach, X. Ni, D. Filonov, A. Slobozhanyuk, A. Alù, and A. B. Khanikaev, Higher-order topological states in photonic kagome crystals with long-range interactions, Nat. Photonics **14**, 89 (2020).
[42] C. Yue, Y. Xu, Z. Song, H. Weng, Y. M. Lu, C. Fang, and X. Dai, Symmetry-enforced chiral hinge states and surface quantum anomalous Hall effect in the magnetic axion insulator $Bi_2C_xSm_xSe_3$, Nat. Phys. **15**, 577 (2019).
[43] Z. Wang, B. J. Wieder, J. Li, B. Yan, and B. A. Bernevig, Higher-Order Topology, Monopole Nodal Lines, and the Origin of Large Fermi Arcs in Transition Metal Dichalcogenides $X\mathrm{Te}_2$ ($X =$ Mo, W), Phys. Rev. Lett. **123**, 186401 (2019).
[44] Y. Xu, Z. Song, Z. Wang, H. Weng, and X. Dai, Higher-Order Topology of the Axion Insulator $EuIn_2As_2$, Phys. Rev. Lett. **122**, 256402 (2019).
[45] R. X. Zhang, F. Wu, and S. Das Sarma, Möbius Insulator and Higher-Order Topology in $MnBi_{2n}Te_{3n+1}$, Phys. Rev. Lett. **124**, 136407 (2020).
[46] Z. Su, Y. Kang, B. Zhang, Z. Zhang, and H. Jiang, Disorder induced phase transition in magnetic higher-order topological insulator: A machine learning study, Chin. Phys. B **28**, 117301 (2019).
[47] C. Wang and X. R. Wang, Disorder-induced quantum phase transitions in three-dimensional second-order topological insulators, Phys. Rev. Research **2**, 033521 (2020).
[48] C. A. Li, B. Fu, Z. A. Hu, J. Li, and S. Q. Shen, Topological Phase Transitions in Disordered Electric Quadrupole Insulators, Phys. Rev. Lett. **125**, 166801 (2020).
[49] A. L. Szabó and B. Roy, Dirty higher-order Dirac semimetal: Quantum criticality and bulk-boundary correspondence, Phys. Rev. Research **2**, 043197 (2020).
[50] J. González, F. Guinea, and M. A. H. Vozmediano, Marginal-Fermi-liquid behavior from two-dimensional Coulomb interaction, Phys. Rev. B **59**, R2474 (1999).
[51] P. Goswami and S. Chakravarty, Quantum Criticality between Topological and Band Insulators in $3+1$ Dimensions, Phys. Rev. Lett. **107**, 196803 (2011).
[52] P. Hosur, S. A. Parameswaran, and A. Vishwanath, Charge Transport in Weyl Semimetals, Phys. Rev. Lett. **108**, 046602 (2012).
[53] E.-G. Moon, C. Xu, Y. B. Kim, and L. Balents, Non-Fermi-Liquid and Topological States with Strong Spin-Orbit Coupling, Phys. Rev. Lett. **111**, 206401 (2013).
[54] B.-J. Yang, E.-G. Moon, H. Isobe, and N. Nagaosa, Quantum criticality of topological phase transitions in three-dimensional interacting electronic systems, Nat. Phys. **10**, 774 (2014).
[55] J. Hofmann, E. Barnes, and S. Das Sarma, Why Does Graphene Behave as a Weakly Interacting System?, Phys. Rev. Lett. **113**, 105502 (2014).
[56] H.-H. Lai, Correlation effects in double-Weyl semimetals, Phys. Rev. B **91**, 235131 (2015).
[57] S.-K. Jian and H. Yao, Correlated double-Weyl semimetals with Coulomb interactions: Possible applications to $HgCr_2Se_4$ and $SrSi_2$, Phys. Rev. B **92**, 045121 (2015).
[58] Y. Huh, E.-G. Moon, and Y. B. Kim, Long-range Coulomb interaction in nodal-ring semimetals, Phys. Rev. B **93**, 035138 (2016).
[59] H. Isobe, B.-J. Yang, A. Chubukov, J. Schmalian, and N. Nagaosa, Emergent Non-Fermi-Liquid at the Quantum

Critical Point of a Topological Phase Transition in Two Dimensions, Phys. Rev. Lett. **116**, 076803 (2016).
[60] G. Y. Cho and E.-G. Moon, Novel quantum criticality in two dimensional topological phase transitions, Sci. Rep. **6**, 19198 (2016).
[61] H. Isobe and N. Nagaosa, Coulomb Interaction Effect in Weyl Fermions with Tilted Energy Dispersion in Two Dimensions, Phys. Rev. Lett. **116**, 116803 (2016).
[62] See Supplemental Material at http://link.aps.org/supplemental/10.1103/PhysRevLett.127.176601 for detailed calculations, which includes Refs. [1,5,18,63–67].
[63] P. Coleman, *Introduction to Many-Body Physics* (Cambridge University Press, Cambridge, 2015).
[64] M. E. Peskin and D. V. Schroeder, *An Introduction to Quantum Field Theory* (CRC Press, Boca Raton, 2019).
[65] A. W. W. Ludwig, M. P. A. Fisher, R. Shankar, and G. Grinstein, Integer quantum Hall transition: An alternative approach and exact results, Phys. Rev. B **50**, 7526 (1994).
[66] A. A. Nersesyan, A. M. Tsvelik, and F. Wenger, Disorder effects in two-dimensional Fermi systems with conical spectrum: Exact results for the density of states, Nucl. Phys. **B438**, 561 (1995).
[67] A. Altland, B. Simons, and M. Zirnbauer, Theories of low-energy quasi-particle states in disordered d-wave superconductors, Phys. Rep. **359**, 283 (2002).
[68] Z. Wang, X.-L. Qi, and S.-C. Zhang, Topological invariants for interacting topological insulators with inversion symmetry, Phys. Rev. B **85**, 165126 (2012).
[69] S.-Q. Shen, W.-Y. Shan, and H.-Z. Lu, Topological insulator and the Dirac equation, SPIN **01**, 33 (2011).
[70] R. Shankar, Renormalization-group approach to interacting fermions, Rev. Mod. Phys. **66**, 129 (1994).
[71] X.-L. Qi, T. L. Hughes, and S.-C. Zhang, Topological field theory of time-reversal invariant insulators, Phys. Rev. B **78**, 195424 (2008).
[72] Z. Wang, X. L. Qi, and S. C. Zhang, Topological Order Parameters for Interacting Topological Insulators, Phys. Rev. Lett. **105**, 256803 (2010).
[73] Z. Wang, X. L. Qi, and S. C. Zhang, Topological invariants for interacting topological insulators with inversion symmetry, Phys. Rev. B **85**, 165126 (2012).
[74] H. Nielsen and M. Ninomiya, β-Function in a non-covariant Yang-Mills theory, Nucl. Phys. **B141**, 153 (1978).
[75] S. Chadha and H. Nielsen, Lorentz invariance as a low energy phenomenon, Nucl. Phys. **B217**, 125 (1983).
[76] M. Sitte, A. Rosch, J. S. Meyer, K. A. Matveev, and M. Garst, Emergent Lorentz Symmetry with Vanishing Velocity in a Critical Two-Subband Quantum Wire, Phys. Rev. Lett. **102**, 176404 (2009).
[77] M. M. Anber and J. F. Donoghue, Emergence of a universal limiting speed, Phys. Rev. D **83**, 105027 (2011).
[78] G. Bednik, O. Pujols, and S. Sibiryakov, Emergent Lorentz invariance from strong dynamics: Holographic examples, J. High Energy Phys. 11 (2013) 64.
[79] S. Sibiryakov, From Scale Invariance to Lorentz Symmetry, Phys. Rev. Lett. **112**, 241602 (2014).
[80] I. V. Kharuk and S. M. Sibiryakov, Emergent Lorentz invariance with chiral fermions, Theor. Math. Phys. **189**, 1755 (2016).
[81] B. Roy, V. Juričić, and I. F. Herbut, Emergent Lorentz symmetry near fermionic quantum critical points in two and three dimensions, J. High Energy Phys. 04 (2016) 018.
[82] A. P. Balachandran and S. Vaidya, Emergent chiral symmetry: Parity and time reversal doubles, Int. J. Mod. Phys. A **12**, 5325 (1997).
[83] D. R. Candido, M. Kharitonov, J. C. Egues, and E. M. Hankiewicz, Paradoxical extension of the edge states across the topological phase transition due to emergent approximate chiral symmetry in a quantum anomalous Hall system, Phys. Rev. B **98**, 161111(R) (2018).
[84] A. L. Szab and B. Roy, Emergent chiral symmetry in a three-dimensional interacting Dirac liquid, J. High Energy Phys. 01 (2021) 004.
[85] L. Balents, M. P. A. Fisher, and C. Nayak, Nodal liquid theory of the pseudo-gap phase of high-Tc superconductors, Int. J. Mod. Phys. B **12**, 1033 (1998).
[86] P. Fendley, K. Schoutens, and J. de Boer, Lattice Models with $\mathcal{N} = 2$ Supersymmetry, Phys. Rev. Lett. **90**, 120402 (2003).
[87] S.-S. Lee, Emergence of supersymmetry at a critical point of a lattice model, Phys. Rev. B **76**, 075103 (2007).
[88] Y. Yu and K. Yang, Supersymmetry and the Goldstino-like Mode in Bose-Fermi Mixtures, Phys. Rev. Lett. **100**, 090404 (2008).
[89] Y. Yu and K. Yang, Simulating the Wess-Zumino Supersymmetry Model in Optical Lattices, Phys. Rev. Lett. **105**, 150605 (2010).
[90] B. Bauer, L. Huijse, E. Berg, M. Troyer, and K. Schoutens, Supersymmetric multicritical point in a model of lattice fermions, Phys. Rev. B **87**, 165145 (2013).
[91] T. Grover, D. N. Sheng, and A. Vishwanath, Emergent space-time supersymmetry at the boundary of a topological phase, Science **344**, 280 (2014).
[92] P. Ponte and S.-S. Lee, Emergence of supersymmetry on the surface of three-dimensional topological insulators, New J. Phys. **16**, 013044 (2014).
[93] S.-K. Jian, Y.-F. Jiang, and H. Yao, Emergent Spacetime Supersymmetry in 3D Weyl Semimetals and 2D Dirac Semimetals, Phys. Rev. Lett. **114**, 237001 (2015).
[94] S.-K. Jian, C.-H. Lin, J. Maciejko, and H. Yao, Emergence of Supersymmetric Quantum Electrodynamics, Phys. Rev. Lett. **118**, 166802 (2017).
[95] P. Feldmann, A. Wipf, and L. Zambelli, Critical Wess-Zumino models with four supercharges in the functional renormalization group approach, Phys. Rev. D **98**, 096005 (2018).
[96] P.-L. Zhao and G.-Z. Liu, Absence of emergent supersymmetry at superconducting quantum critical points in dirac and Weyl semimetals, npj Quantum Mater. **4**, 37 (2019).
[97] G. Volovik, Emergent physics: Fermi-point scenario, Phil. Trans. R. Soc. A **366**, 2935 (2008).
[98] S. L. Sondhi, S. M. Girvin, J. P. Carini, and D. Shahar, Continuous quantum phase transitions, Rev. Mod. Phys. **69**, 315 (1997).

[99] M. Imada, A. Fujimori, and Y. Tokura, Metal-insulator transitions, Rev. Mod. Phys. **70**, 1039 (1998).
[100] D. T. Son, Quantum critical point in graphene approached in the limit of infinitely strong Coulomb interaction, Phys. Rev. B **75**, 235423 (2007).
[101] M. S. Foster and I. L. Aleiner, Graphene via large N: A renormalization group study, Phys. Rev. B **77**, 195413 (2008).
[102] M. Levin and A. Stern, Fractional Topological Insulators, Phys. Rev. Lett. **103**, 196803 (2009).
[103] J. Maciejko, X.-L. Qi, A. Karch, and S.-C. Zhang, Fractional Topological Insulators in Three Dimensions, Phys. Rev. Lett. **105**, 246809 (2010).
[104] T. Neupert, L. Santos, C. Chamon, and C. Mudry, Fractional Quantum Hall States at Zero Magnetic Field, Phys. Rev. Lett. **106**, 236804 (2011).
[105] N. Regnault and B. A. Bernevig, Fractional Chern Insulator, Phys. Rev. X **1**, 021014 (2011).
[106] H. Wei, S.-P. Chao, and V. Aji, Excitonic Phases from Weyl Semimetals, Phys. Rev. Lett. **109**, 196403 (2012).
[107] S. Rachel, Interacting topological insulators: A review, Rep. Prog. Phys. **81**, 116501 (2018).
[108] S.-Y. Xu, Y. Xia, L. A. Wray, S. Jia, F. Meier, J. H. Dil *et al.*, Topological phase transition and texture inversion in a tunable topological insulator, Science **332**, 560 (2011).